ADVANCED REENTRY AEROMECHANICS. VOLUME II. AERODYNAMIC SHATTERING OF ICE CRYSTALS IN HYPERSONIC FLIGHT

Girard A. Simons

Physical Sciences, Incorporated

Prepared for:

Air Force Office of Scientific Research
Space and Missile Systems Organization

April 1975

PSI TR-22

ADVANCED REENTRY AEROMECHANICS

INTERIM SCIENTIFIC REPORT

VOLUME II

AERODYNAMIC SHATTERING OF ICE CRYSTALS IN HYPERSONIC FLIGHT

by

Girard A. Simons

April, 1975

Jointly Sponsored by

The Space and Missile Systems Organization

and

The Air Force Office of Scientific Research (AFSC)

Contract F44620-74-C-0022

PHYSICAL SCIENCES INC.
18 Lakeside Office Park
Wakefield, MA 01880

ABSTRACT

A theoretical study of ice crystal/shock layer interaction has been carried out in order to assess the relative kinetic energy of an ice crystal upon impact with a hypersonic vehicle. A dynamic fracture criterion has been developed which predicts the size of the ice crystal fragments formed at the vehicle bow shock. An analysis of the ice crystal breakup predicts that the outer fragments continue to shatter and prevent the shock layer gas from penetrating the fragment cloud. The fragment cloud is then treated as a deformable fluid drop, and the reduced impact velocity due to lateral spreading is determined.

Conditions of Reproduction

TABLE OF CONTENTS

LIST OF ILLUSTRATIONS

I. INTRODUCTION

As a supersonic or hypersonic vehicle passes through a real atmosphere, it may encounter relatively large clouds of dust, rain or ice. A great deal of attention has previously been given to the problems of dust[1] and rain[2-11], but not until recently has significant effort been devoted to the interaction of ice crystals with the shock layer. Wu[12] has studied the melting and vaporization of an ice crystal in a hypersonic shock layer and demonstrated a significant reduction in particle size and impact velocity for ice crystals initially of the order of 10μ diameter. Larger crystals were ralatively unaffected by melting and vaporization. In the same report, Teare[12] demonstrated that ice crystals may shatter at the vehicle bow-shock. This introduces the possibility that the fractured ice crystal or "fragment cloud" may deform as it passes through the vehicle shock layer. This deformation will be lateral to the relative gas velocity and will tend to increase the drag area of the fragment cloud. Hence, the velocity of the fragment cloud will decrease more rapidly than that of a rigid particle, and the velocity with which the fragment cloud impacts the vehicle may be significantly lower than that with which a "rigid" ice crystal would impact the vehicle.

To study this phenomenon we must first develop a criterion for the dynamic fracture of the ice crystal at the vehicle shock. This is carried out in section II. The problem of ice crystal breakup is addressed in section III, and in section IV we examine the dynamics of the fragment cloud and demonstrate the reduced impact velocity due to the lateral deformation of the cloud.

The dynamic shattering criterion used in section II is subject to the experimental verification. However, the dynamics of the fragment cloud are insensitive to the actual shattering process and the results of section IV are only weakly dependent on the dynamic shattering criterion.

II. INITIAL FRACTURE OF THE ICE CRYSTAL

A) Conditions for Fracture

A schematic of an ice crystal entering a hypersonic shock layer is given in Fig. 1. The ice crystal enters the vehicle shock layer with velocity U_∞, finds itself moving with supersonic velocity relative to the shock layer gas and thereby generates its own bow shock or crystal shock. Only the normal component of the shock Mach number is important for the pressure loading on the crystal. The pressure loading as a function of normal Mach number M_x can be calculated with the aid of Fig. 2. The subscript x represents conditions upstream of the vehicle shock and subscript y denotes conditions in the vehicle shock layer. The Mach number of the ice crystal relative to the shock layer gas is

$$M_I = \frac{v_x - v_y}{a_y} = M_y \left(\frac{v_x}{v_y} - 1 \right)$$

which may be determined from the normal shock tables. The pressure P_s is the total pressure behind a shock of Mach number M_I moving into a gas of pressure P_y. Thus, P_s may also be obtained from the normal shock relations. The static yield criterion[13] indicates that fracture will occur in the vehicle shock layer if the radius of Mohr's circle, $(P_s - P_y)/2$, is greater than S_s, the yield stress of ice in shear.

$$P_s - P_y \geq 2\, S_s$$

If the speed of sound in the ice, a_o, is greater than V_x, the ice crystal will

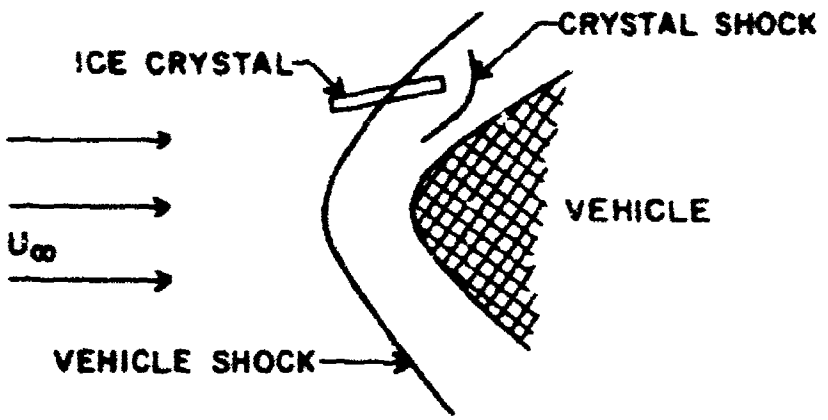

Fig. 1 Ice Crystal-Shock Wave Interaction

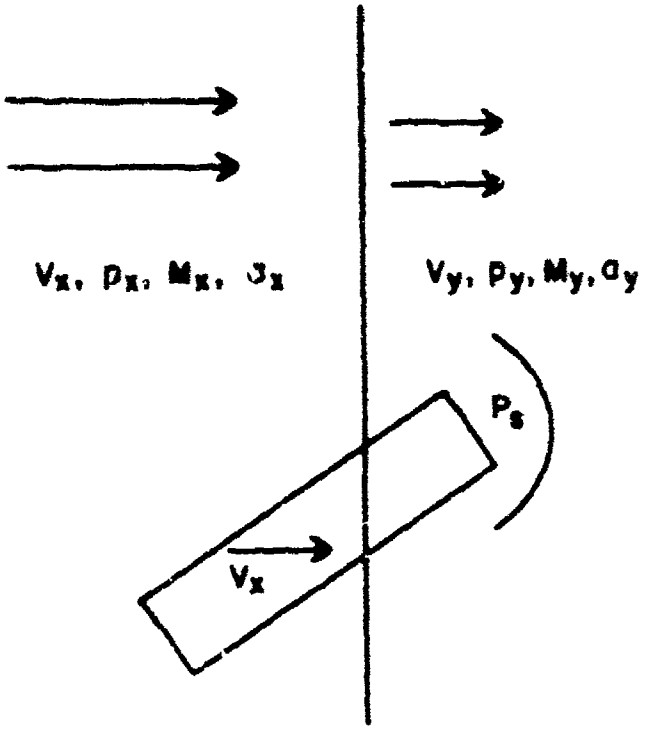

Fig. 2 Pressure Loading on Crystal

shatter upstream of the vehicle shock if

$$P_s - P_x \geq 2 S_s.$$

This fracture criterion is illustrated in Fig. 3 and demonstrates that most hypersonic vehicles will shatter ice crystals through the bow shock wave - ice crystal interaction process outlined above. However, this conclusion is based on the application of a static yield criterion. We must proceed to develop a model for the dynamic fracture of a brittle material under impulsive loading.

B) Dynamic Fracture Criterion

Ice crystals passing the bow shock wave of a hypersonic vehicle are subject to very short duration impulsive loads, and a consistent dynamic yield criterion must be established in order to analyze the shattering problem. First, we define three different times relevant to dynamic loads. τ_D is the duration of the applied load, τ_T is the transient time for application of the load ($\tau_T \leq \tau_D$) and τ_R is the response time or the time required for a specimen of length L to know a load has been applied. Clearly, $\tau_R = L/a_o$, where a_o is the speed of sound in the specimen.

By definition, static loading occurs when $\tau_T \gg \tau_R$ and the static yield stress (σ_s) is the appropriate measure of the maximum load that the specimen can tolerate without plastic deformation or failure. Clearly, when $\tau_T \ll \tau_R$, a dynamic yield stress (σ_D) is a necessary measure of failure. When $\tau_T = O(\tau_R)$ we assert that $\sigma_D = O(\sigma_s)$.

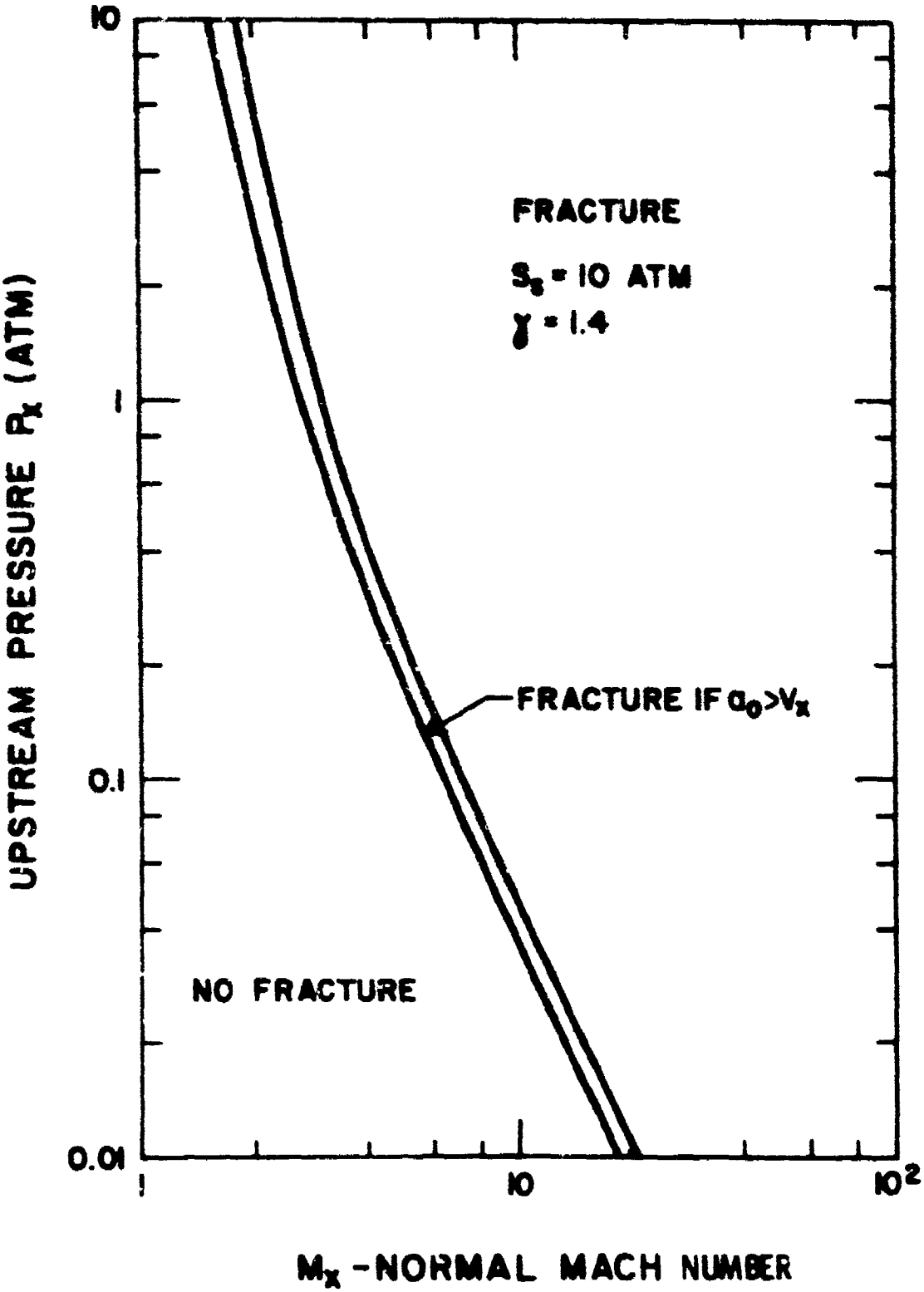

Fig. 3 Conditions for Fracture

One example of a situation where $\tau_T = \tau_R$ is a monochromatic stress wave. Let X_x be the longitudinal stress (tension or compression) in a stress wave

$$X_x = A_k \sin(\pi k a_o t) \cos(\pi k x).$$

For an element of length $1/k$, $\tau_R = \tau_T = \left(\frac{1}{k a_o}\right)$. Therefore, failure occurs when $A_k = 0\ (\sigma_s)$. An alternate way of looking at the stress wave is in terms of the particle velocities, U_x. The momentum equation

$$\rho \frac{\partial U_x}{\partial t} = X_x$$

yields

$$U_x = \frac{a_o A_k}{E} \cos(\pi k a_o t) \sin(\pi k x)$$

where E is young's modulus relating stress (σ) to strain (e) $\left(\sigma = Ee \text{ and } a_o = \sqrt{E/\rho}\right)$. If we interpret U_x as a series of elements of length $1/k$ colliding with velocity $a_o A_k / E$, then impact theory[14] indicates that failure occurs when the impact velocity exceeds $C\ (e_s a_o)$. Since $\sigma_s = E e_s$, this criteria reduces to $A_k = 0\ (\sigma_s)$

Having developed a rational argument for applying a static yield criterion to the monochromatic stress wave, we now make the following bold hypothesis which, while plausible, can be justified only if the subsequent conclusions agree with experiment.

HYPOTHESIS: Dynamic Yield Stress may be obtained by Fourier expanding the applied load and applying the monochromatic yield criterion to each wave. Failure occurs when $A_k = Q\,\sigma_s$ where Q is O (1) and is to be determined by applying this technique to an impulsively loaded specimen.

The primary argument against this hypothesis is that the single monochromatic wave may in no way represent the total stress which is the sum of all the waves. While this is true, one could assert that a specimen of length L would be fractured by its primary mode and that a small segment (length ℓ) of the specimen would be shattered by the primary mode associated with the length ℓ, even though the primary mode of the small segment would be a higher order mode of the larger specimen. Hence, it is within this context that we apply the monochromatic yield criterion to each Fourier component of a dynamic load. While we cannot theoretically confirm the basic hypothesis, we proceed with the intention of verifying it through empirical confirmation of the conclusions which are subsequent to the basic hypothesis.

C) One-Dimensional Fracture

Let us first examine the present theory by applying it to the problem of a one-dimensional slab of thickness b that is impulsively loaded on one side with pressure P_s for time τ_D. The load is impulsively removed at the end of that time interval ($\tau_D \ll b/a_o$). A schematic of the loading and unloading waves in (x, t) coordinates is given in Fig. 4. If we stand at some

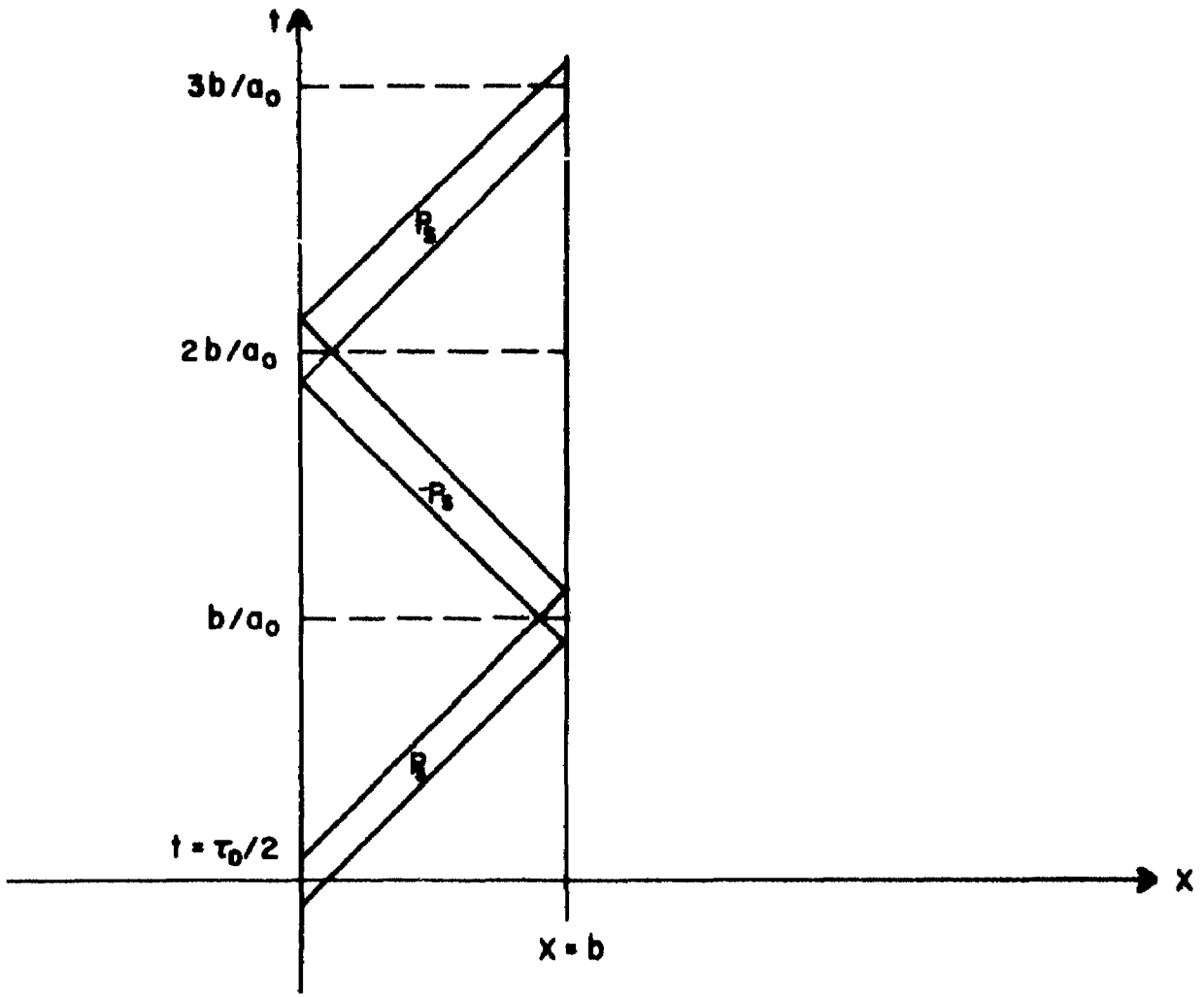

Fig. 4 Wave Diagram of Impulsive Short Term Load

position x between $a_o \tau_D/2$ and $b - a_o \tau_D/2$, the time dependent force on an element is shown in Fig. 5. The Fourier expansion of X_x is given by

$$X_x = \sum_n \frac{4P_s}{n\pi} \sin\left(\frac{n\pi a_o \tau_D}{2b}\right) \sin\left(\frac{n\pi a_o t}{b}\right) \sin\left(\frac{n\pi x}{b}\right).$$

The dynamic fracture criterion indicates that the primary mode (n = 1) will fracture the specimen if

$$\frac{4P_s}{\pi} \sin\left(\frac{\pi a_o \tau_D}{2b}\right) \approx \frac{2P_s a_o \tau_D}{b} > Q\sigma_s$$

or

$$P_s > \left(\frac{Qb}{2a_o \tau_D}\right)\sigma_s \ .$$

Hence, the dynamic yield stress σ_D is given by

$$\sigma_D = \left(\frac{Qb}{2a_o \tau_D}\right)\sigma_s \qquad \text{for } \tau_D \ll b/a_o$$

and illustrates that σ_D is inversely proportional to τ_D and indeed is in excess of σ_s provided that Q is of order unity.

To determine the value of Q, let us again take a one-dimensional slab and impulsively load it in tension (T) for all time. The wave diagram is illustrated in Fig. 6 and the pressure-time history is shown in Fig. 7. The corresponding Fourier series representation of the dynamic load is given by

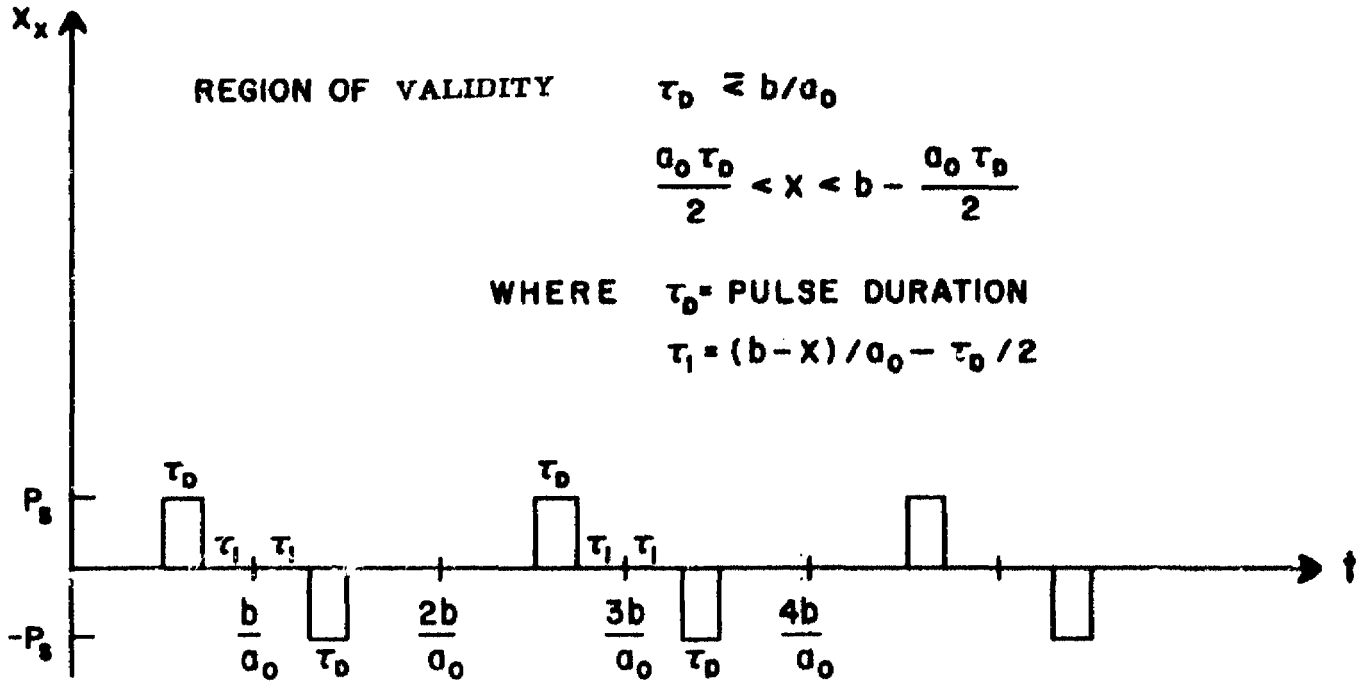

Fig. 5 Pressure "Trace" For Impulsive Short Term Load

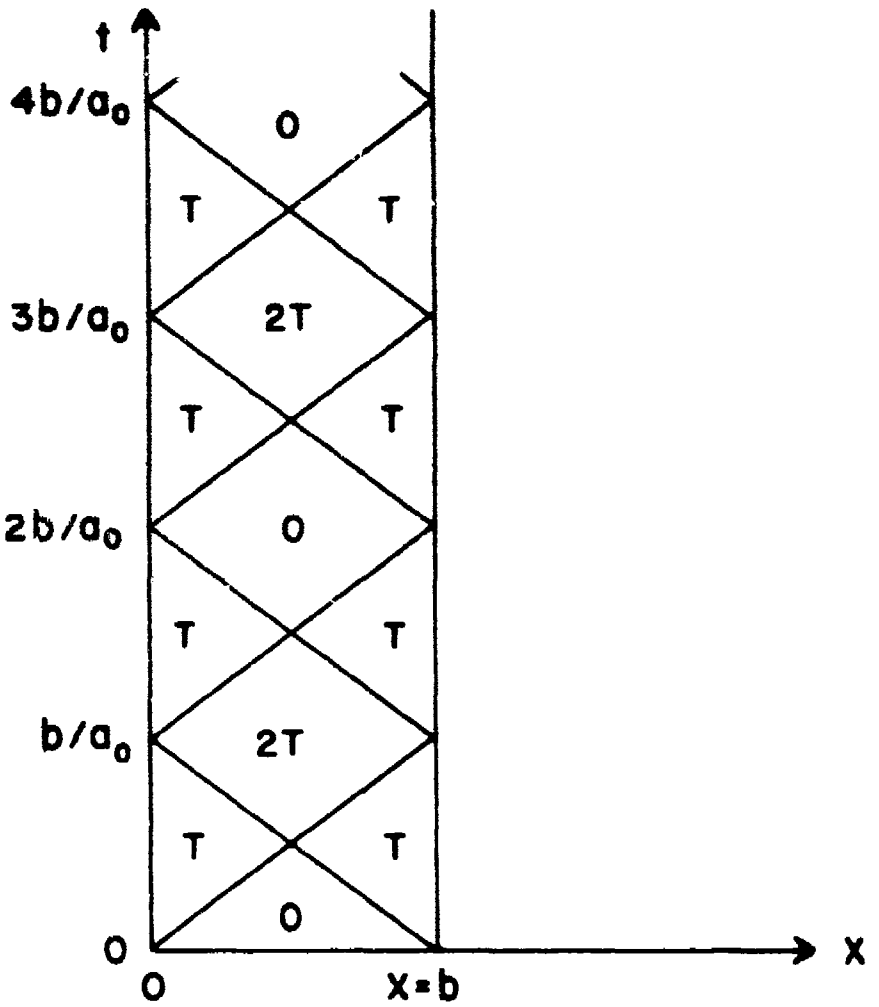

Fig. 6 Wave Diagram For Impulsive Load in Tension

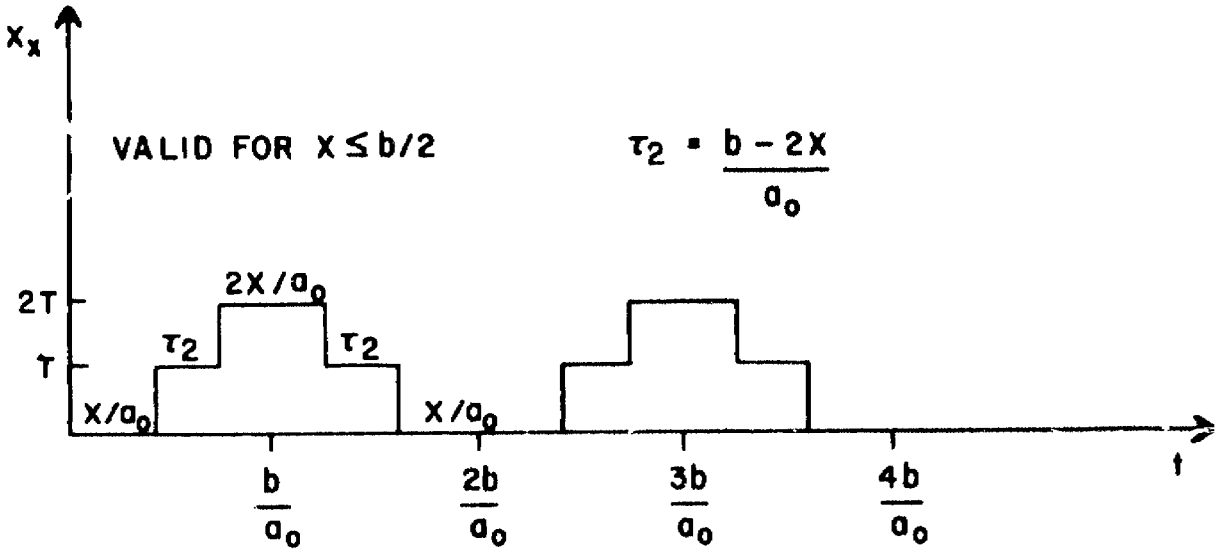

Fig. 7 Pressure "Trace" For Impulsive Load in Tension

$$X_x = T + \sum_n \frac{2T}{n\pi}\left(\cos n\pi - 1\right)\sin\left(\frac{n\pi x}{b}\right)\cos\left(\frac{n\pi a_o t}{b}\right).$$

An impulsively applied load creates twice the strain as a slowly applied load.[15] Thus, the impulsive load will fracture the specimen when T is only $\sigma_s/2$. Equating the amplitude of the n = 1 mode of the above expansion to $Q\sigma_s$, we determine

$$Q_{1D} \equiv \frac{4}{\pi} . \qquad (1)$$

Note that we have obtained Q by comparing the amplitude of standing waves. Any subsequent use of the value of Q must be made with standing waves. A completely consistent approach could be developed using traveling waves but the values of Q would differ by a factor of 2.

Having developed a criterion for fracture of a dynamically loaded specimen, let us now examine shattering. Consider a one-dimensional slab impulsively loaded on one side and held constant for all time. This is the one-dimensional analogue of the ice crystal loading at the bow shock of a hypersonic vehicle. The Fourier expansion of the dynamic load is expressed as

$$X_x = \sum_n - \frac{2P_s}{n\pi}\cos\left(\frac{n\pi a_o t}{b}\right)\sin\left(\frac{n\pi x}{b}\right) + P_s\left(1 - x/b\right).$$

Suppose $P_s \gg \sigma_s$. Then, not only can the n = 1 mode fracture the specimen, but the n = 2 mode can break those fragments and so on up to the critical

value of n (n_c) where the nth mode is just strong enough to fracture the specimen. This value of n is determined by

$$\frac{2 P_s}{n_c \pi} = Q \sigma_s$$

or

$$n_c = \frac{P_s}{\sigma_s}$$

and the corresponding size of the fragments (ℓ) of the n_c mode is given by

$$\ell = \frac{b}{n_c} = \left(\frac{\sigma_s}{P_s}\right) b \quad .$$

These are the largest fragments that can survive the applied pressure P_s. Smaller fragments can exist due to the shattering by other modes. That is, the n_cth mode fractures the specimen at values of x/b equal to

$$\frac{x}{b} = \frac{1}{2 n_c}, \frac{3}{2 n_c}, \frac{5}{2 n_c}, \frac{7}{2 n_c} \text{ - - - - - - - - - - } \frac{2 n_c - 1}{2 n_c} \quad .$$

The n_c-1 mode fractures the specimen at

$$\frac{x}{b} = \frac{1}{2 (n_c - 1)}, \frac{3}{2 (n_c - 1)}, \frac{5}{2 (n_c - 1)}, \frac{7}{2 (n_c - 1)} \text{ - - - } \frac{2 (n_c - 1) - 1}{2 (n_c - 1)} \quad .$$

The largest fragment is then

$$\frac{\Delta x}{b} = \frac{3}{2 n_c} - \frac{1}{2 n_c} = \frac{1}{n_c}$$

whereas the smallest is

$$\frac{\Delta x}{b} = \frac{1}{2(n_c - 1)} - \frac{1}{2n_c} \approx \frac{1}{2n_c^2}$$

Therefore, for one-dimensional shattering, we have determined that the fragment sizes range from the smallest

$$\ell_{min} = \frac{1}{2}\left(\frac{\sigma_s}{P_s}\right)^2 b$$

to the largest, ℓ_{max}

$$\ell_{max} = \left(\frac{\sigma_s}{P_s}\right) b \qquad (2)$$

Since the ice crystal erosion problem is dominated by the large crystals, we shall study the two-dimensional and three-dimensional shattering problems with the understanding that the characteristic fragment size refers to the largest fragments, and that smaller fragments can exist.

D. High Frequency Limitations

The results of section C) places no upper limit on the frequency of the fracturing wave or, equivalently, place no lower limit on the size of the shattered fragments. It is well known[16] that the minimum wave length that can exist in a solid is of the order of the lattice spacing (s) and the maximum frequency is the photon frequency ω_p

$$\omega_p \approx a_o/s$$

where a_o is the speed of sound in the specimen. These concepts may be included in the shattering analysis by adding some "inertia" to the stress tensor. Assuming

$$\sigma = E(e + \beta \dot{e})$$

where $\dot{e}$ is $\frac{\partial e}{\partial t}$ and both E and β are constants, the momentum equation becomes

$$\rho \frac{\partial^2 U}{\partial t^2} = \frac{\partial \sigma}{\partial x} = E \frac{\partial^2 U}{\partial x^2} + E\beta \frac{\partial^3 U}{\partial t \partial x^2} .$$

Solving the initial value problem,

$$U(x,t) = \sin\left(\frac{2\pi x}{\lambda}\right) e^{-\omega t}$$

for λ real and ω complex we see that propagation cannot exist above the frequency $2/\beta$ or below the wavelength $\pi a_o \beta$. Hence, it follows that

$$\beta \approx \frac{1}{\omega_p} \approx \frac{s}{a_o} .$$

Solving the boundary value problem,

$$U(x,t) = e^{-x/\delta_e} e^{i(\omega t - 2\pi x/\lambda)}$$

for ω, λ and the decay depth δ_e all real, we obtain

$$\delta_e \approx \frac{2a_o}{\omega^2 \beta} \approx \frac{a_o^2}{s\omega^2}$$

where δ_e approaches s as ω approaches ω_p.

For an applied load of arbitrary frequency ω, caution must be taken to insure that $\delta_e > L$ before using the proposed dynamic yield criterion since it omits skin depth effects. For an impulsively loaded specimen of length L,

the frequency corresponding to the n'th mode is

$$\omega \approx \frac{n a_o}{L} .$$

Validity of the shattering analysis requires

$$\delta_e > L$$

or $$L > n^2 s$$

or $$\ell_{max} > ns$$

and $$\ell_{min} > s$$

Thus, the ice crystal shattering analysis is valid down to fragment sizes of the order of s. High frequency effects do not influence the shattering by an impulsively applied load but may become important for high frequency loads and large test specimens.

E. Two-Dimensional Fracture

The one-dimensional shattering analysis is readily extended to two dimensions by expanding the applied load into a double Fourier series. Suppose we have a two-dimensional ice crystal with pressure P_s impulsively applied at one end. The applied pressure may be expanded as a square wave over the lateral dimension (a) of the ice crystal

$$P_s(y) = \frac{2 P_s}{\pi} \sum_m \left(\frac{1 - \cos m\pi}{m} \right) \sin \left(\frac{m \pi y}{a} \right) .$$

The one-dimensional plane wave solution was given by

$$X_x = \sum_n \frac{-2 P_s(y)}{n\pi} \cos \left(\frac{n \pi a_o t}{b} \right) \sin \left(\frac{n \pi x}{b} \right)$$

where a_o was $\sqrt{E/\rho}$ and $P_s(y)$ was constant. Thus, the plane wave representation of an end loaded two-dimensional ice crystal is given by

$$X_x = \sum_m \sum_n \frac{-4\,P_s\,(1-\cos m\pi)}{mn\pi^2} \sin\left(\frac{m\pi y}{a}\right) \sin\left(\frac{n\pi x}{b}\right) \cos\left(\frac{n\pi a_o t}{b}\right)$$

or, in standing wave form

$$X_x = \sum_m \sum_n \frac{-2\,P_s\,(1-\cos m\pi)}{m\pi^2} \cos\left(\frac{n\pi a_o t}{b}\right)$$

$$\cdot \left[\cos\left\{\frac{n\pi x}{b} - \frac{m\pi y}{a}\right\} - \cos\left\{\frac{n\pi x}{b} + \frac{m\pi y}{a}\right\}\right] \qquad (3)$$

Similarly, we take a two-dimensional specimen and impulsively load it in tension T for all time.

$$X_x = \sum_m \sum_n \frac{2\,T\,(1-\cos m\pi)\,(\cos n\pi - 1)}{mn\pi^2} \cos\left(\frac{n\pi a_o t}{b}\right)$$

$$\cdot \left[\cos\left\{\frac{n\pi x}{b} - \frac{m\pi y}{a}\right\} - \cos\left\{\frac{n\pi x}{b} + \frac{m\pi y}{a}\right\}\right]$$

Just as in the one-dimensional case, failure occurs when the tension T exceeds one half of its static limit. Therefore, the coefficient relating the wave amplitude to the yield stress is

$$Q_{2D} \equiv \frac{4}{\pi^2} \quad . \qquad (4)$$

The value of Q_{2D} is not restricted to a particular failure mode. The

maximum tension T may be limited by either shear or tension. In obtaining Eq. (4), it was stated only that the impulsive load is twice as strong as the static load. The primary mode, whose amplitude is $8T/\pi^2$, will break when T is "1/2". Hence, Q_{2D} is $4/\pi^2$.

For an axial load such as that applied to the ice crystal, Mohr's circle predicts that the maximum shear (S) occurs at

$$y = \pm x + \text{constant}$$

and is of strength

$$S = \frac{X_x}{2} \quad .$$

Examining Eq. (3), we see that the strength of the (m, n) mode is a maximum along

$$y = \pm \left(\frac{a}{b}\right)\left(\frac{n}{m}\right)x + \text{constant}$$

Therefore, the natural mode selection that would maximize the shear stress on the wave is

$$\frac{a}{b} \equiv \frac{m}{n} \quad .$$

Under the constraint of $b \geq a$, hence $n \geq m$, the shear stress on the two-dimensional ice crystal may be expressed as

$$S = \frac{-P_s (1-\cos m\pi) a}{m^2 \pi^2 b} \cos\left(\frac{m\pi a_o t}{a}\right) \left[\cos\left\{\frac{m\pi}{a}\left(x-y\right)\right\}\right.$$

$$\left. -\cos\left\{\frac{m\pi}{a}\left(x+y\right)\right\}\right]$$

The dynamic fracture criterion predicts failure for the critical value of m, denoted by m_c. Equating the wave amplitude of S to $Q_{2D} S_s$,

$$\frac{2 P_s a}{m_c^2 \pi^2 b} = S_s Q_{2D} \text{ for } (b \geq a),$$

the value of m_c becomes

$$m_c = \sqrt{\left(\frac{P_s}{2 S_s}\right)\left(\frac{a}{b}\right)}, \quad \left(\frac{P_s}{2 S_s} \geq \frac{b}{a}\right). \tag{5}$$

Note: for $m_c < 1$, we must use the one-dimensional results of Section C, otherwise the lateral dimension of the fragment is greater than a. The results are continuous if it is assumed that the maximum axial stress is limited by the shear mode ($\sigma_s = 2 S_s$). The characteristic fragment size is a/m_c or

$$\ell_{2D} = \sqrt{\left(\frac{2 S_s}{P_s}\right)\left(\frac{a}{b}\right)} \quad \text{for} \quad \left(\frac{P_s}{2 S_s} \geq \frac{b}{a}\right) \text{ or } (\ell < a),$$

and

$$\ell_{1D} = \left(\frac{\sigma_s}{P_s}\right) b \text{ for } \left(\frac{P_s}{2 S_s} \leq \frac{b}{a}\right) \text{ or } (\ell > a). \tag{6}$$

Hence, the two-dimensional shattering analysis is appropriate only if the fragment size is less than the small dimension of the initial crystal. Otherwise, shattering is one-dimensional along the length of the specimen.

F. Three-Dimensional Shattering

Suppose that we now have a three-dimensional crystal of length b

and base area a^2 ($b \geq a$). Expanding the applied force in a triple Fourier series, the amplitude of the wave would be inversely proportional to the mode number cubed.

$$A_{n,m,q} \sim \frac{P_s}{nmq}$$

where

$$\frac{n}{b} = \frac{m}{a} = \frac{q}{a}$$

or

$$A_{n,m,q} \approx \frac{P_s a}{m^3 b}$$

Applying the dynamic fracture criterion to the amplitude of the wave, we obtain

$$\frac{P_s a}{m_c^3 b} \sim S_s$$

or

$$m_c \approx \left(\frac{P_s}{S_s}\right)^{1/3} \left(\frac{a}{b}\right)^{1/3} .$$

The fragment size is a/m_c or

$$\ell_{3D} = \left(\frac{2S_s}{P_s}\right)^{1/3} \left(a^2 b\right)^{1/3} \text{ for } \left(\frac{P_s}{2S_s} \geq \frac{b}{a}\right) , \qquad (7)$$

where the constant was chosen to be continuous with the one-dimensional results when $\ell_{3D} = a$. For $\ell_{3D} > a$, we again use the one dimensional result.

$$\ell_{1D} = \left(\frac{\sigma_s}{P_s}\right) b \text{ for } \left(\frac{P_s}{2S_s} \leq \frac{b}{a}\right) .$$

Hence, the three-dimensional analysis is appropriate only if the fragment size is less than a. Otherwise, shattering is one-dimensional along the length of the specimen.

III. ICE CRYSTAL BREAKUP

A) Description of the Model

As the fractured ice crystal passes through the vehicle shock layer, it will breakup and deform by the action of the shock layer gas. The deformation of the fragment cloud is studied in section IV. However, on a time scale small with respect to the cloud deformation time, ice crystal breakup must be assessed in order to determine the appropriate model for the fragment cloud. That is, does the fragment cloud behave as a separate fluid, a two phase flow or as a fluidized bed?

To begin to answer this question, we see from Section II-B that the maximum velocity imparted to the solid particle is

$$U_{max} = \frac{a_o A_k}{E} = \frac{a_o P_s}{E} .$$

Since $a_o \sim 3$ km/sec, $E \sim 10^5$ atm and $P_s \sim 10^3$ atm (max), we obtain

$$U_{max} \sim 30 \text{m/sec}$$

The expansion Mach number (relative to the gas) corresponding to U_{max} would be 0.1 upstream of the vehicle shock and 0.01 downstream of the shock. Hence, the expansion is much too slow to be thought of as an "explosion". Rather, we think of it as a "convective separation" where the crystal fragments separate with some characteristic velocity indicative of the initial fracturing process. As the fragments separate, shock layer gas will influx through the cracks as shown in Figure 8. The time scale for gas to penetrate the fragment cloud is short compared to the time required

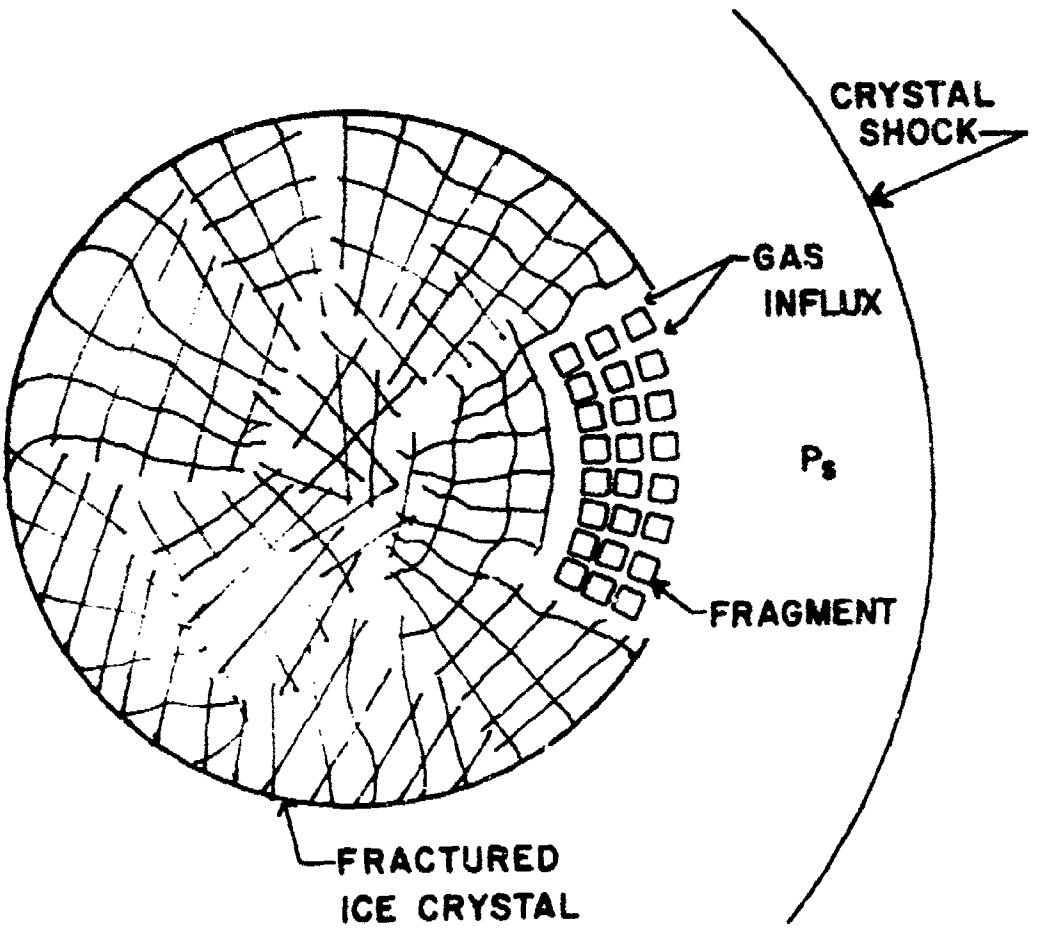

Fig. 8 Ice Crystal Breakup

for the fragment to respond dynamically to the gas. In fact, the latter time scale is the deformation time and this is the distinction between crystal breakup and cloud deformation.

As the gas penetrates through the cracks, the gas seeks pressure equilibrium ($\nabla P \rightarrow 0$). However, the pressure difference across a fragment is $\Delta \nabla P$, which, if in excess of σ_s, will fracture the fragment. Continuous fracturing of the fragments would increase the surface/volume of the solid and prevent further influx of gas. If the incoming gas achieves pressure equilibrium within the fragment cloud before further fracturing can occur, the fragment cloud must be treated as a two phase flow. However, if further fracturing prevents the gas from penetrating the fragment cloud, the cloud may be thought of as a separate gas which deforms in much the same way that a liquid drop deforms. In the following sections, it is shown that the fragment cloud may be treated as a separate fluid which deforms as a continuous medium.

B) Formulation of the Model

Investigating the stagnation region of the fragment cloud, we assume that the velocity of the fragments is radial with magnitude increasing linearly in r

$$U_r = \left(\frac{a_o P_s}{E}\right)\left(\frac{r}{R_o}\right)$$

where R_o is the initial radius of the fragment cloud or ice crystal. If the fragments expand without slowing down

$$r(t) = r(o)\left(1 + \frac{a_o P_s t}{E R_o}\right)$$

where r(o) is the independent coordinate r and r(t) is the coordinate of the fragment that was initially at r. The porous volume within the fragment cloud may be expressed as

$$V_p = \left(\frac{4}{3}\pi r^3(t) - \frac{4}{3}\pi r^3\right)\frac{\Omega}{4\pi}$$

where Ω is the solid angle subtended by the stagnation area. For $t << R_o/U_{max}$,

$$V_p = \frac{\Omega a_o P_s t}{E R_o} r^3 .$$

$$dV_p = A_p dr \tag{8}$$

and

$$A_p = \frac{3\Omega a_o P_s t r^2}{E R_o}$$

The equations of motion for the gas are written using a control volume fixed to the fragments. It is assumed that the velocity of the fragments is constant in time and small with respect to the gas velocity.

Gas Continuity:

$$\frac{\partial}{\partial r}\left(\bar{\rho}\bar{u}A_p\right)dr = -\frac{\partial}{\partial t}\left(\bar{\rho}dV_p\right)$$

Gas Momentum:

$$\frac{\partial}{\partial t}\left(\bar{\rho}\bar{u}\,dV_p\right) + \frac{\partial}{\partial r}\left(\bar{\rho}\bar{u}^2A_p\right)dr = -A_p\frac{\partial\bar{p}}{\partial r}dr - FdA_s \quad NdA_n$$

where $\bar{\rho}$ is the gas density, $\bar{u}$ the gas velocity and $\bar{p}$ is the gas pressure. The shear force between the fragments and the gas is denoted by F and the

normal pressure force is denoted by N.

To determine F, consider the incompressible flow between parallel plates separated by distance 2h

$$u = u_{\mathfrak{C}} (h^2 - y^2)/h^2$$

where y is measured from the centerline, equidistant between the plates. The average gas velocity $\bar{u}$ is related to $u_{\mathfrak{C}}$ by continuity

$$\bar{u} = \int_{-h}^{h} u \left(\frac{dy}{2h}\right) = \frac{2}{3} u_{\mathfrak{C}} .$$

The shear stress F is determined from

$$F = \bar{\mu} \left.\frac{\partial u}{\partial y}\right|_{-h} = \frac{2u_{\mathfrak{C}}\bar{\mu}}{h} = \frac{3\bar{u}\bar{\mu}}{h}$$

where $\bar{\mu}$ is the gas viscosity.

To determine h(r,t), note that the porous volume per fragment is $6h\ell^2$ where ℓ is the fragment size. The number of fragments in volume element $\Omega r^2 dr$ is $\Omega r^2 dr/\ell^3$. Therefore, the porous volume element is

$$dV_p = \left(6h\ell^2\right)\left(\frac{\Omega r^2 dr}{\ell^3}\right)$$

Comparing to eq (8), we obtain h.

$$h = \frac{a_o P_s \ell t}{2ER_o}$$

The surface area of each fragment is $6\ell^2$. Thus, the net surface area in volume element $\Omega r^2 dr$ is

$$dA_s = 6\ell^2 \left(\frac{\Omega r^2 dr}{\ell^3}\right)$$

and

$$FdA_s = \frac{36\bar{\mu}\,\bar{u}\,ER_o\Omega r^2 dr}{\ell^2 a_o P_s t}$$

The normal pressure force N is

$$N = \frac{1}{2}\,\bar{\rho}\,\bar{u}^2\,\text{sign}(\bar{u}).$$

The normal surface area associated with each fragment is $2h\ell$. Thus,

$$dA_n = 2h\ell\left(\frac{\Omega r^2 dr}{\ell^3}\right)$$

or

$$NdA_n = \frac{a_o P_s t \bar{\rho}\,\bar{u}^2 \text{sign}(\bar{u})\Omega r^2 dr}{2ER_o\ell}$$

Using V_p, A_p, FdA_s and NdA_n, the continuity and momentum equations become, respectively,

$$\frac{t}{r^2}\frac{\partial}{\partial r}\left(\bar{\rho}\,\bar{u}\,r^2\right) + \frac{\partial}{\partial t}\left(t\bar{\rho}\right) = 0 \qquad (9)$$

and

$$\bar{\rho}\,\frac{\partial\bar{u}}{\partial t} + \bar{\rho}\,\bar{u}\,\frac{\partial\bar{u}}{\partial r} + \frac{\partial\bar{p}}{\partial r} + \frac{12\,\bar{u}\,\bar{\mu}E^2R_o^2}{a_o^2 P_s^2 \ell^2 t^2} + \frac{\bar{\rho}\,\bar{u}^2}{6\ell}\,\text{sign}(\bar{u}) = 0. \qquad (10)$$

The fragment size ℓ appearing in eq. (10) is a time dependent quantity which is yet to be determined. If we apply a pressure gradient across a crystal fragment, that fragment will fracture when

$$\ell\,\frac{\partial\bar{p}}{\partial r} > \sigma_s.$$

The shattering theory indicates that the fragment will break into smaller fragments of size $\left(\sigma_s / \ell\,\frac{\partial\bar{p}}{\partial r}\right)^{1/3}$ ℓ in a time scale of order ℓ/a_o.

Therefore

$$\frac{D\ell}{Dt} \doteq \frac{\partial \ell}{\partial t} = -\left(\frac{\ell - \left(\frac{\sigma_s}{\ell \frac{\partial \bar{p}}{\partial r}} \right)^{1/3} \ell}{(\ell / a_o)} \right)$$

or

$$\frac{\partial \ell}{\partial t} = -a_o \left[1 - \left(\frac{\sigma_s}{\ell \frac{\partial \bar{p}}{\partial r}} \right)^{1/3} \right] \tag{11}$$

Equations (9), (10) and (11) represent three equations in the four unknowns $\bar{\rho}$, $\bar{u}$, $\bar{p}$ and ℓ. In the next two sections, they are solved by specifying $\bar{\rho}$ in the incompressible and sonic limits.

C) Incompressible Solution

In the incompressible limit, the continuity equation yields $\bar{u}$,

$$\bar{u} = -r/3t$$

and the momentum equation yields $\bar{p}$ (ℓ, r, t)

$$\frac{\partial \bar{p}}{\partial r} = \frac{4\bar{\mu} E^2 R_o^2 r}{a_o^2 P_s^2 \ell^2 t^3} - \frac{4\bar{\rho} r}{9t^2} + \frac{\bar{\rho} r^2}{54 \ell t^2} \tag{12}$$

Substituting $\frac{\partial \bar{p}}{\partial r}$ into the shattering relation, eq. (11), yields

$$\frac{\partial (\ell/\ell_o)}{\partial \tau} = -1 + \left[\frac{\epsilon_o^3 \left(\frac{r}{R_o} \right)}{\left(\frac{\ell}{\ell_o} \right) \tau^3} + \frac{\epsilon_1^3 \left(\frac{r}{R_o} \right)^2}{\tau^2} - K^3 \epsilon_1^3 \frac{\left(\frac{\ell}{\ell_o} \right) \left(\frac{r}{R_o} \right)}{\tau^2} \right]^{-1/3} \tag{13}$$

where $\ell_o = \left(\frac{\sigma_s}{P_s}\right)^{1/3} R_o$

$$\tau = t/(\ell_o/a_o)$$

$$Rey = \frac{\bar{\rho} a_o R_o}{\bar{\mu}}$$

$$\epsilon_o = \left(\frac{4\bar{\rho}}{\rho}\right)^{1/3}\left(\frac{1}{Rey}\right)^{1/3}\left(\frac{E}{P_s}\right)^{2/9}\left(\frac{E}{\sigma_s}\right)^{7/9}$$

$$\epsilon_1 = \left(\frac{\bar{\rho}}{\rho}\right)^{1/3} P_s^{2/9} E^{1/3} \Big/ (54)^{1/3} (\sigma_s)^{5/9}$$

$$K = (24)^{1/3}\left(\frac{\sigma_s}{P_s}\right)^{1/9}$$

For the ice cyrstal/shock layer interaction problem, we are interested in the following range of values.

$$Rey = 10^4 \text{ to } 10^5$$

$$P_s = 10 \text{ atm to } 10^3 \text{ atm}$$

$$\sigma_s \doteq 10 \text{ atm}$$

$$\rho \doteq 100\,\bar{\rho}$$

$$E \doteq 10^5 \text{ atm}$$

Figure 9 illustrates that our range of interest (cross hatched region) lies in the domain where $\epsilon_o >> \epsilon_1, \epsilon_o >> K\epsilon_1$, and $\epsilon_o >> 1$. Thus, for r near R_o, equation (13) becomes

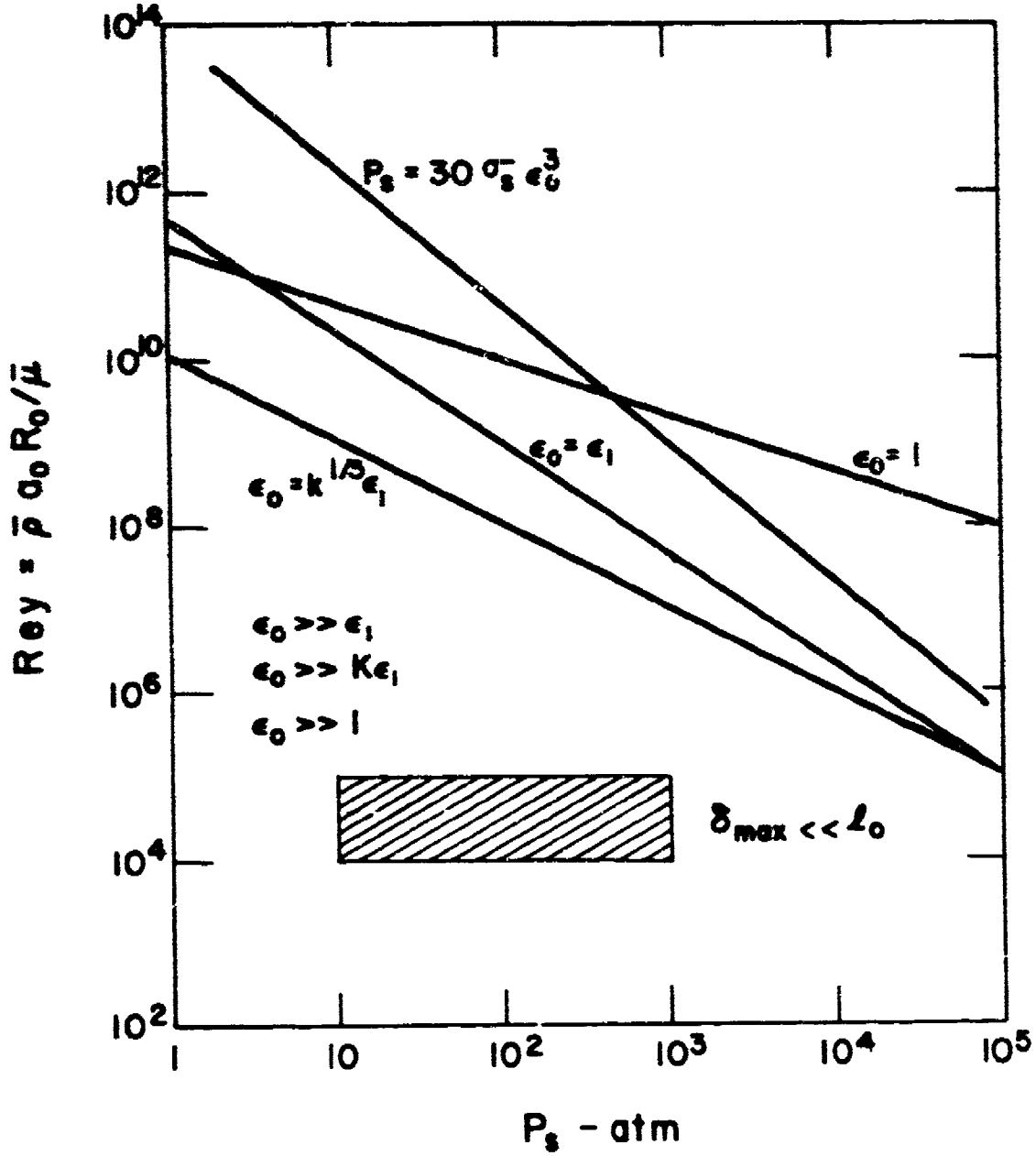

Fig. 9 Ordering Of The Shattering Equation (Incompressible Flow)

$$\frac{\partial(\ell/\ell_o)}{\partial\tau} = -1 + \frac{\left(\frac{\ell}{\ell_o}\right)^{1/3}\tau}{\epsilon_o} \quad . \tag{14}$$

The nature of equation (14) depends on the size of ϵ_o. For $\epsilon_o << 1$, shattering will stop at some value of ℓ near ℓ_o (shattering stops when $\frac{\partial \ell}{\partial \tau} = 0$ or when $\ell = 0$). However, for the case of interest, ($\epsilon_o >> 1$) the approximate solution to (14) is

$$\frac{\ell}{\ell_o} \doteq 1 - \tau \tag{15}$$

for $\tau \leq 1$ ($\ell = 0$ for $\tau \geq 1$). Thus, continuous shattering at $r = R_o$ breaks the outer fragments into tiny fragments which will prevent further penetration by the shock layer gas.

To estimate the penetration distance of the shock layer gas, we assume that the pressure gradient at $r = R_o$ is continuous over the penetration distance, δ.

$$\delta = P_s / \left(\frac{\partial \bar{p}}{\partial r}\right) \quad \left(\delta_{max} << R_o\right) \tag{16}$$

From (15) and (12), the pressure gradient is expressed in terms of dimensionless parameters previously defined.

$$\frac{\partial \bar{p}}{\partial r} = \frac{\epsilon_o^{\,3}\sigma_s}{\ell_o \tau^3 (1-\tau)^2} \qquad (r \approx R_o)$$

The penetration distance becomes

$$\frac{\delta}{\ell_o} = \frac{P_s \tau^3 (1-\tau)^2}{\epsilon_o^{\,3}\sigma_s}$$

or

$$\frac{\delta_{max}}{\ell_o} \doteq \frac{P_s}{300\sigma_s \epsilon_o^3}$$

For the range of parameters illustrated in Figure 9, δ_{max} is much less than ℓ_o. Thus, the shock layer gas does not penetrate the fragment cloud, and the fragment cloud may be treated as a separate gas or incompressible fluid without surface tension.

D) Sonic Solution

The gas flux into the porous regions of the fragment cloud is more likely to be sonic than incompressible. Rewriting the shattering equation for $\bar{u} = \bar{u}^*$, we obtain

$$\frac{\partial\left(\frac{\ell}{\ell_o}\right)}{\partial\tau} = -1 + \left[\frac{\epsilon_2^3}{\left(\frac{\ell}{\ell_o}\right)\tau^2} + \frac{P_s}{6\sigma_s}\right]^{-1/3} \qquad (17)$$

where we assumed

$$\bar{\rho}\,\bar{u}^*\bar{u}^* = P_s$$

and

$$\epsilon_2 = \left(\frac{12}{Rey}\right)^{1/3}\left(\frac{\bar{u}^*}{a_o}\right)^{1/3}\left(\frac{\bar{\rho}}{\rho}\right)^{1/3} \frac{E}{\sigma_s^{2/3} P_s^{1/3}}.$$

For $\bar{u}^* = a_o$ and the range of parameters indicated in Section C), Figure 10 illustrates that the ϵ_2^3 term in eq. (17) is dominant.

$$\frac{\partial\left(\ell/\ell_o\right)}{\partial\tau} \doteq -1 + \frac{\left(\frac{\ell}{\ell_o}\right)^{1/3}\tau^{2/3}}{\epsilon_2}$$

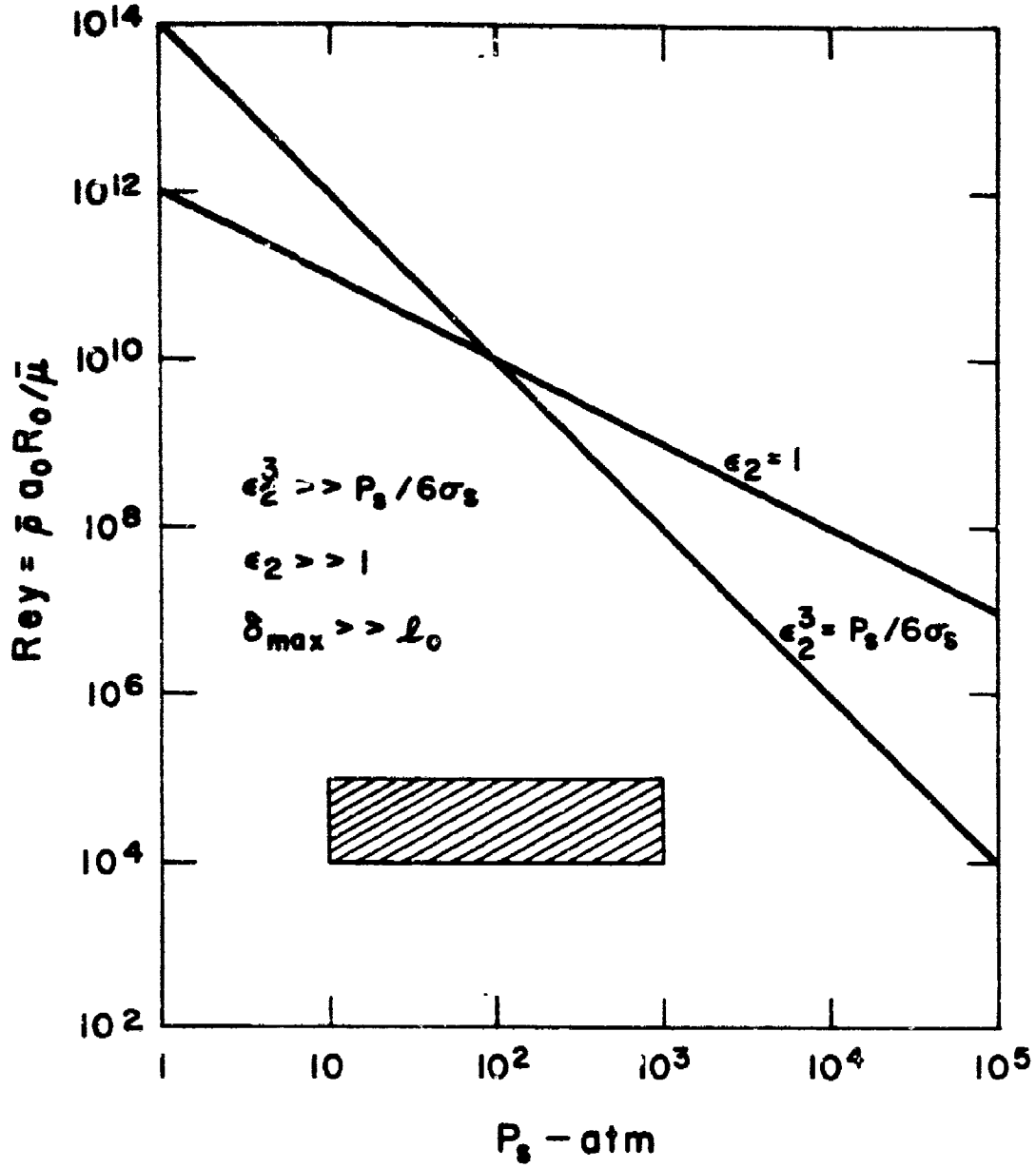

Fig. 10 Ordering Of the Shattering Equation (Sonic Flow)

For $\epsilon_2 >> 1$,

$$\frac{\ell}{\ell_o} \doteq 1 - \tau$$

and the pressure gradient is expressed as

$$\frac{\delta \bar{p}}{\delta r} = \frac{\epsilon_2^3 \sigma_s}{\ell_o \tau^2 (1-\tau)^2} \tag{18}$$

The penetration depth of the shock layer gas is determined from eqs. (16) and (18)

$$\frac{\delta}{\ell_o} = \frac{P_s \tau^2 (1-\tau)^2}{\epsilon_2^3 \sigma_s}$$

or

$$\frac{\delta_{max}}{\ell_o} = \frac{P_s}{16 \epsilon_2^3 \sigma_s} .$$

For the range of parameters indicated in figure 10, $\delta_{max} << \ell_o$. The shock layer gas does not penetrate the fragment cloud and the fragment cloud may be treated as a separate gas or incompressible fluid without surface tension.

IV. FRAGMENT CLOUD MOTION

A) Model For the Cloud Motion

The analysis of the ice crystal breakup indicates that we may treat the fragment cloud as a liquid drop without surface tension. We treat only the mean deformation of the cloud, and any consideration of aerodynamic stripping or catastrophic breakup is omitted. When a liquid drop is out of dynamic equilibrium with a gas, the stagnation pressure will tend to flatten the liquid drop, increase its drag area and cause it to accelerate faster than a rigid particle. This effect would tend to slow down shattered ice crystals that penetrate the shock layer of a hypersonic vehicle and thereby help "shield" the vehicle from ice erosion.

To model this effect, we extend an approach used by Reinecke and Waldman[5] in their rain drop studies. Writing the drop's momentum equation lateral to the relative gas velocity, Reinecke and Waldman[5] use a moment method to develop an equation for the lateral deformation. Assuming that the lateral liquid velocity is linear in the lateral coordinate, they obtain

$$\Delta \frac{d^2\Delta}{dT^2} + 2\left(\frac{d\Delta}{dT}\right)^2 = 4C_p$$

where

$$\Delta = R/R_o \text{ or } D/D_o$$

$$T = \frac{u_2 t \sqrt{\epsilon}}{D_o}$$

u_2 = initial relative gas velocity

ϵ = gas density/liquid density = $\bar{\rho}/\rho$

C_p = pressure coefficient at Raindrop Stagnation Point

The Reinecke and Waldman approach is limited to times for which the relative velocity u is approximately equal to its initial value u_2. Defining the dimensionless relative velocity v

$$v = u/u_2$$

we extend the Reinecke-Waldman equation to include a time dependent relative wind

$$\Delta \frac{d^2\Delta}{dT^2} + 2 \left(\frac{d\Delta}{dT}\right)^2 = 4C_p v^2 \qquad (19)$$

and express the dynamics of u

$$\rho\left(\frac{4}{3}\pi R_o^3\right) \frac{du}{dt} = -\frac{1}{2} \bar{\rho} u^2 C_D \pi R^2$$

or

$$\frac{dv}{dT} = - \left(\frac{3C_D}{4}\right)\sqrt{\epsilon}\ \Delta^2 v^2 \qquad (20)$$

A simultaneous solution to eqs. (19) and (20) is needed to determine the slowdown and lateral spreading of the deformable, incompressible drop.

B) Early and Late Time Solutions

To obtain a solution eqs. (19) and (20), it is natural to seek an early time solution of the form

$$v = v_o + \sqrt{\epsilon}\ v_1 - - - - \qquad \text{as } \epsilon \to 0$$

$$\Delta = \Delta_o + \sqrt{\epsilon}\ \Delta_1 - - - - \qquad \text{as } \epsilon \to 0$$

where

$$\Delta_o = \sqrt{2C_p}\ T + \text{constant (Reinecke-Waldman Result)}$$

and

$$v_o = 1.$$

Obtaining the next order term in v,

$$v = 1 - \sqrt{\epsilon}\ \frac{1}{2}\ C_D C_p T^3 - - - -$$

we note that the expansion is singular when both T and Δ are 0 ($\epsilon^{-1/6}$).

Rescaling the problem to "late time", we define

$$\Sigma = \epsilon^{1/6} T$$

$$\Gamma = \epsilon^{1/6} \Delta$$

and the equations become

$$\Gamma \frac{d^2\Gamma}{d\Sigma^2} + 2\left(\frac{2\Gamma}{d\Sigma}\right)^2 = 4 C_p v^2 \tag{21}$$

$$\frac{dv}{d\Sigma} = -\left(\frac{3C_D}{4}\right) v^2 \Gamma^2. \tag{22}$$

The early time solution provides the initial conditions to (21) and (22).

$$v(0) = 1$$

$$\Gamma(0) = 0 \text{ as } \epsilon \to 0$$

$$\frac{d\Gamma}{d\Sigma} = \sqrt{2C_p}$$

Numerical solutions for $v(\Sigma)$ and $\Gamma(\Sigma)$ are illustrated in Figures 11 and 12 respectively. Over the time scale Σ, a substantial deviation from v = 1 is noted. The decrease in v is enhanced by the deformation of the drop. This deformation causes the liquid drop to accelerate more rapidly than a rigid particle.

If we imagine a shock tube experiment where a stationary liquid drop is suddenly exposed to a relative wind u_2, the drop displacement (x_{ST}) in the shock tube becomes

$$\frac{dx_{ST}}{dt} = u_2 - u \tag{23}$$

In the "Reinecke-Waldman Coordinate", we nondimensionalize to D_o

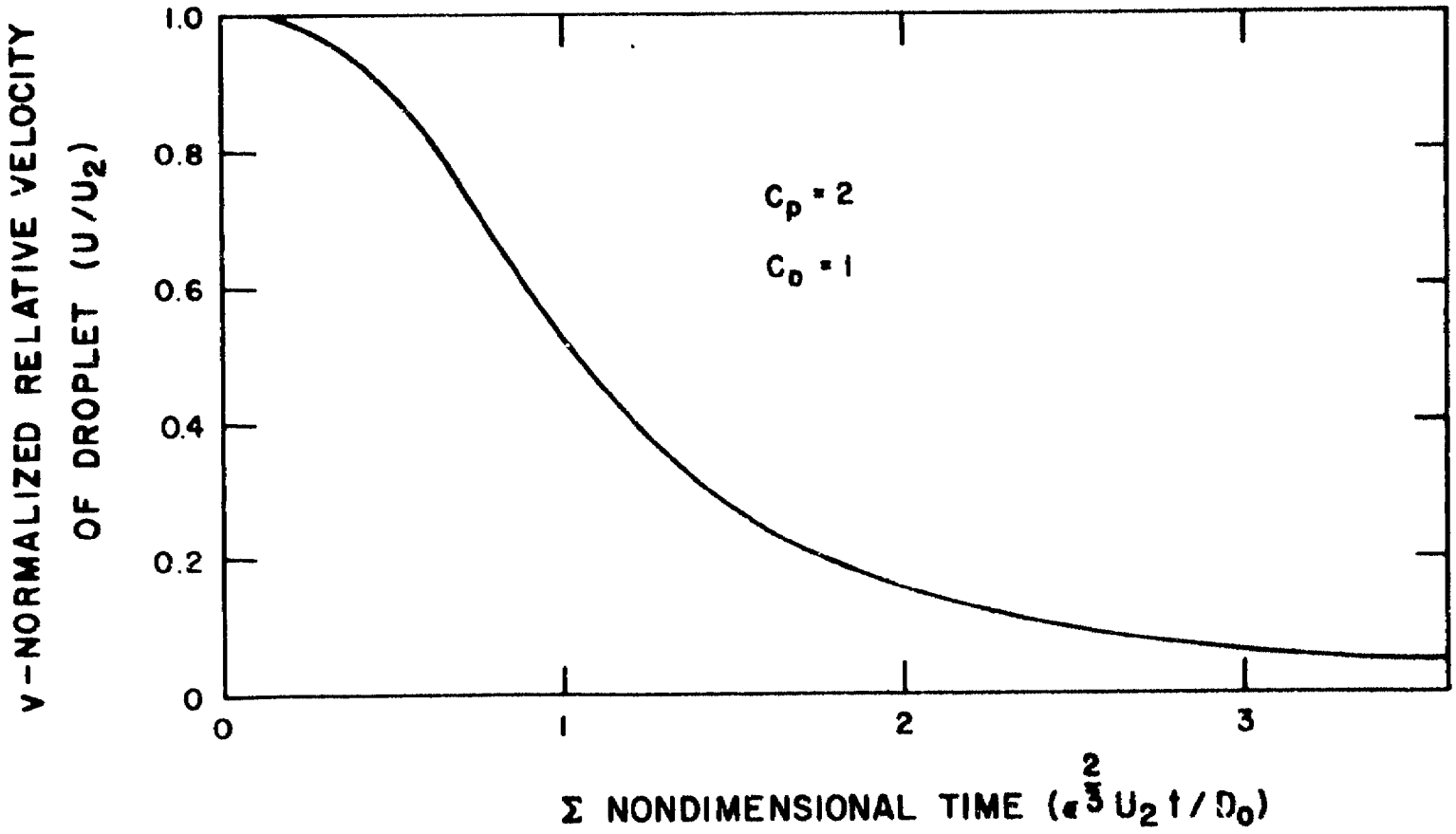

Fig. 11 Late Time Solution For The Relative Velocity

Fig. 12 Late Time Solution For The Lateral Deformation

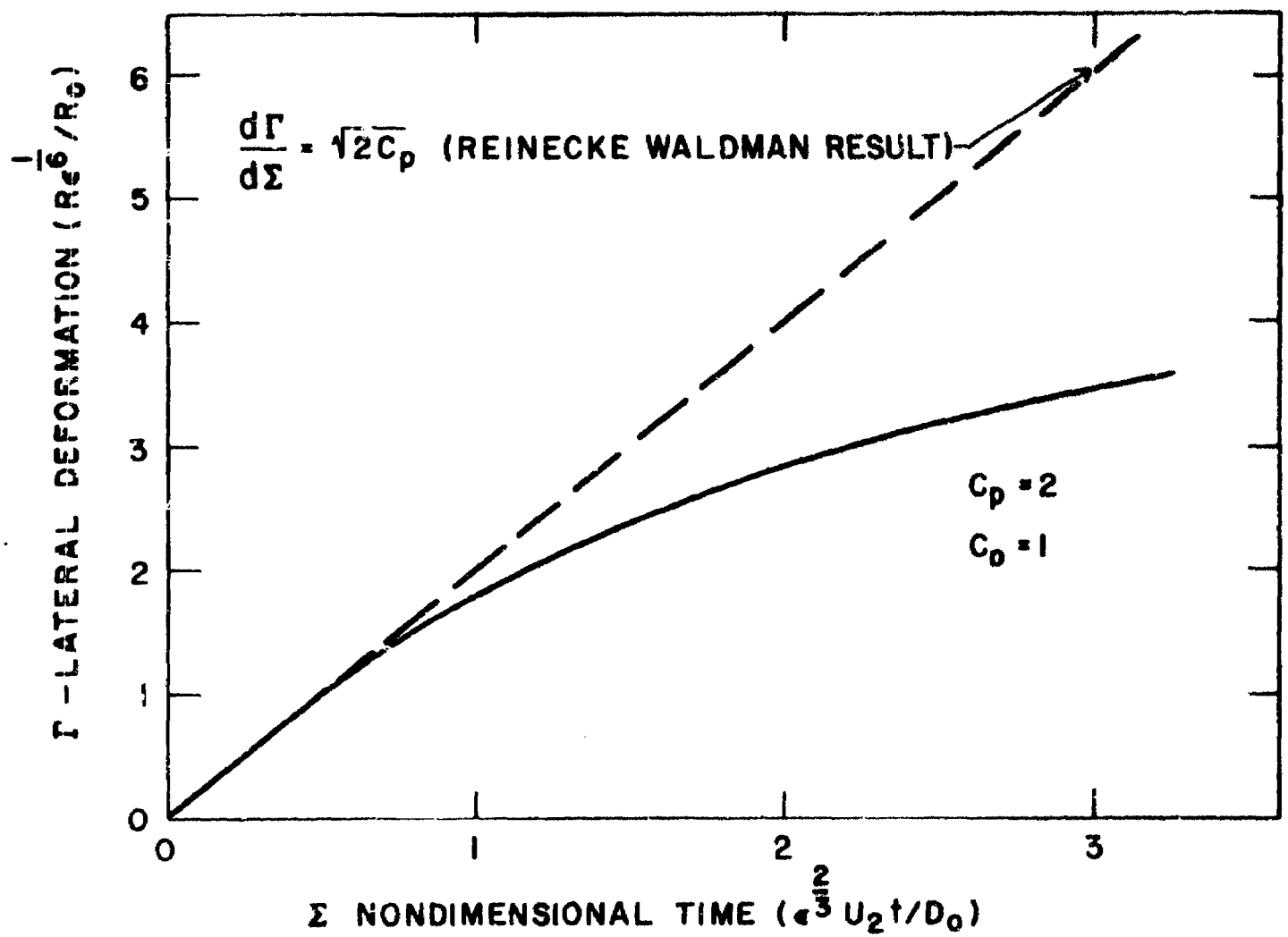

$$X_{ST} = x_{ST} / D_o$$

whereas in the present coordinates, X_{ST} is re-scaled by $\epsilon^{2/3}$

$$Y_{ST} = \epsilon^{2/3} X_{ST}$$

Eq. (23) becomes

$$\frac{dY_{ST}}{d\sum} = 1 - v \qquad (24)$$

A numerical solution of eq. (24) (coupled to (21) and (22)) is illustrated in Figure 13. The results illustrate a very rapid acceleration at small time. Making a small $\sum$ expansion of (21), (22) and (24), we obtain

$$\Gamma = \sqrt{2C_p}\sum$$

$$v = 1 - \frac{1}{2} C_D C_p \sum^3$$

and

$$Y_{ST} = \frac{1}{8} C_D C_p \sum^4$$

Rescaling to the Reinecke-Waldman coordinates

$$X_{ST} = \frac{1}{8} C_D C_p T^4 \qquad \text{(Liquid Drops)}$$

whereas, for solid particles, we integrate eq. (20) with $\Delta \equiv 1$.

$$X_{ST} \doteq \frac{3}{8} C_D T^2 \qquad \text{(Solid Particles)}$$

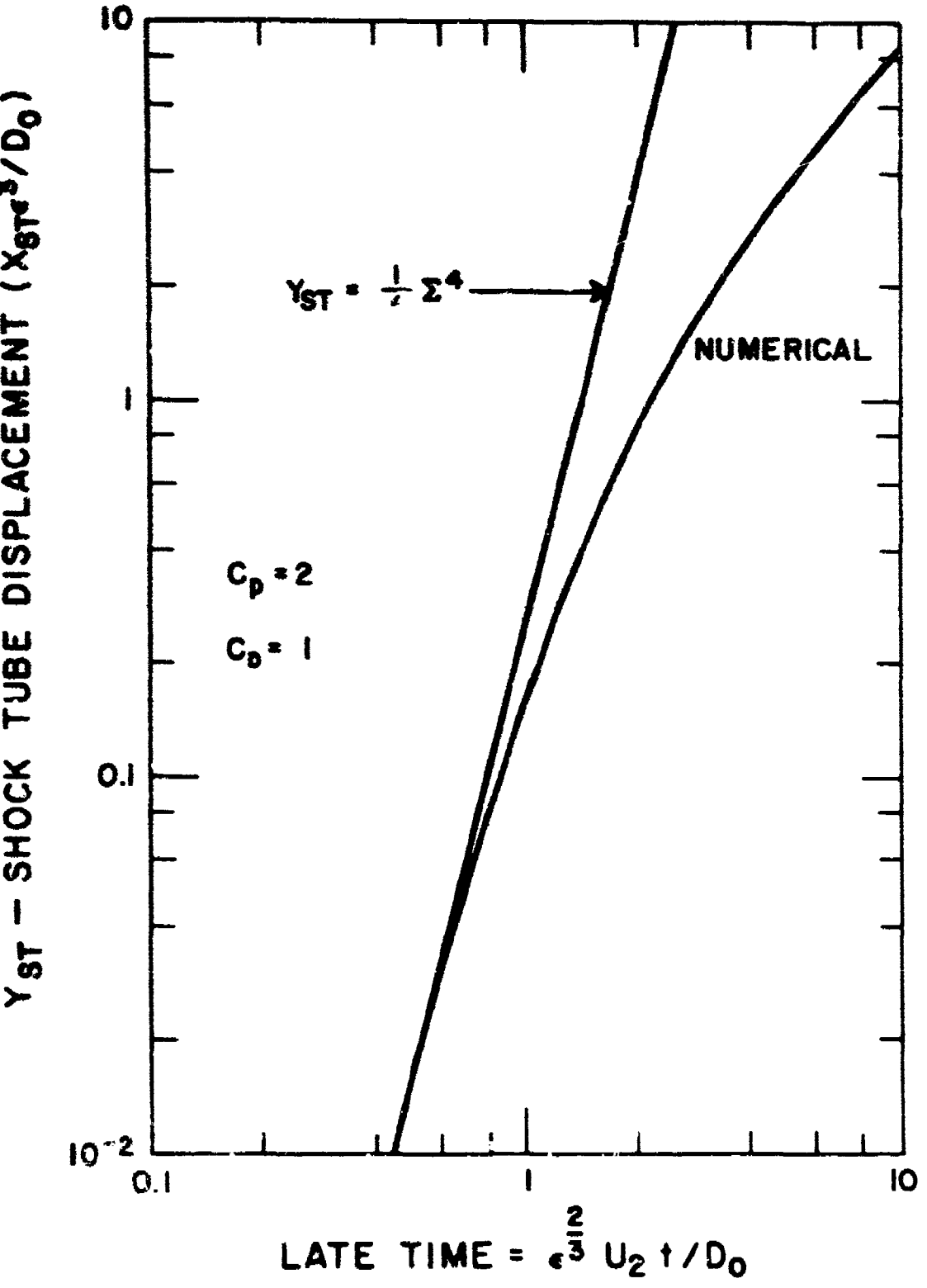

Fig. 13 Late Time Solution For The Shock Tube Displacement

Thus, the acceleration of a liquid drop is significantly different from that of a solid particle and the difference in demonstrated empirically in Figure 14. Recent data of Reinecke and Waldman[11] together with that of Engel[2] closely follows the T^4 curve except for $X_{ST} > 10$, where the T^4 results must yield to the numerical solution. Slightly smaller values of C_p or C_D would yield even better agreement with the data.

C) Application to Stagnation Point Erosion

Having developed a model for the dynamics of a deformable, incompressible fragment cloud, we will now apply the theory to the stagnation point of a hypersonic vehicle and determine the conditions under which the shattering of the ice crystal into a fragment cloud will help shield the vehicle from ice erosion.

Considering the stagnation point shock layer to be a static gas, the penetration (x_{sp}) of the fragment cloud into the shock layer may be written as

$$\frac{dx_{sp}}{dt} = u$$

or

$$\frac{dY_{sp}}{d\sum} = v. \qquad (25)$$

Coupling eqs. (25) to eqs. (21) and (23), numerical results are illustrated in Figure 15. Figures 11 and 15 may be used to determine $v(x_{sp})$. At $x_{sp} = \Delta_s$, the shock stand off distance, v represents v_I, the relative velocity at impact, and v_I^2 represents the relative kinetic energy at impact.

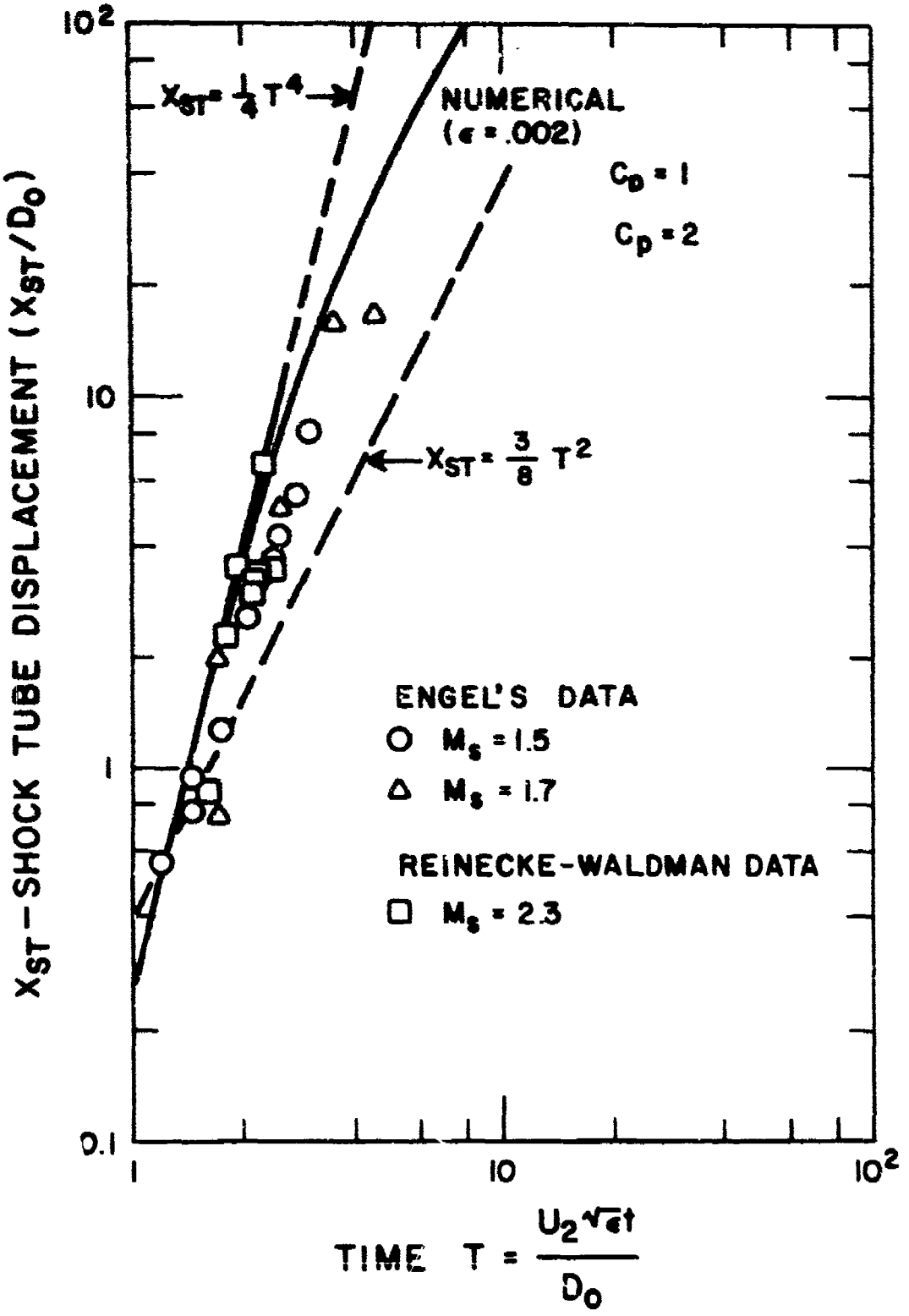

Fig. 14 Dynamics Of Liquid Drops

Fig. 15 Penetration Of a Fragment Cloud Into The Stagnation Point Shock Layer

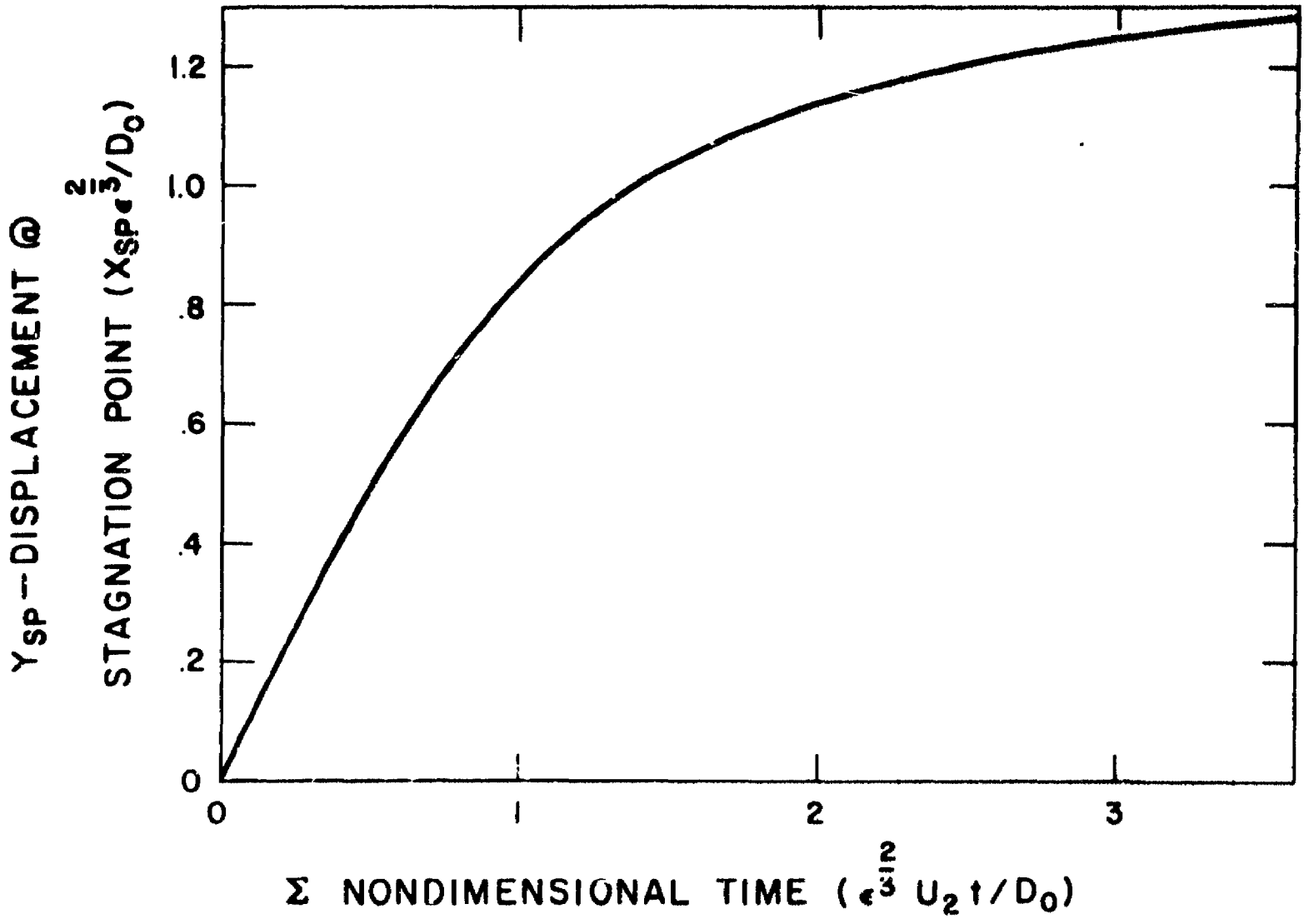

To determine v_I^2 for a solid particle, use Eq. (20) with $\Delta = 1$ ($D = D_o$).

$$\frac{dv}{dT} = -\left(\frac{3C_D}{4}\right)\sqrt{\epsilon}\ v^2 \ .$$

Integration yields

$$v = \left(1 + \frac{3C_D\sqrt{\epsilon}\ T}{4}\right)^{-1}$$

and

$$\frac{x_{sp}}{D_o} = \frac{4}{3\epsilon C_D} \ln\left(1 + \frac{3C_D\sqrt{\epsilon}\ T}{4}\right) \ .$$

At $x_{sp} = \Delta_s$, $v = v_I$, therefore

$$v_I^2 = \exp\left(-3C_D \epsilon \Delta_s \quad \right). \qquad \text{(Rigid Particles)}$$

The relative impact kinetic energy of solid particles is compared to that of a fragment cloud of the same initial size in Fig. 16. The results indicate that the smallest size fragment cloud that will not cause damage to a hypersonic vehicle may be an order of magnitude greater than the minimum tolerable rigid particle. A specific case treated by Wu[12] is illustrated in Fig. 17 and compared to the present results. Wu compared the results for a rigid particle to that for the melting, vaporizing particle and showed that the critical size for causing damage was above 10 μ. When ice crystal shattering is accounted for, the vehicle under consideration can tolerate up to 50 μ diameter crystals. The shielding effect obviously increases rapidly with increasing nose radius. Consideration of fragment

cloud melting, vaporization, stripping and Taylor instability should further increase the minimum tolerable size ice crystal.

Fig. 16 Impact Energy At Stagnation Point

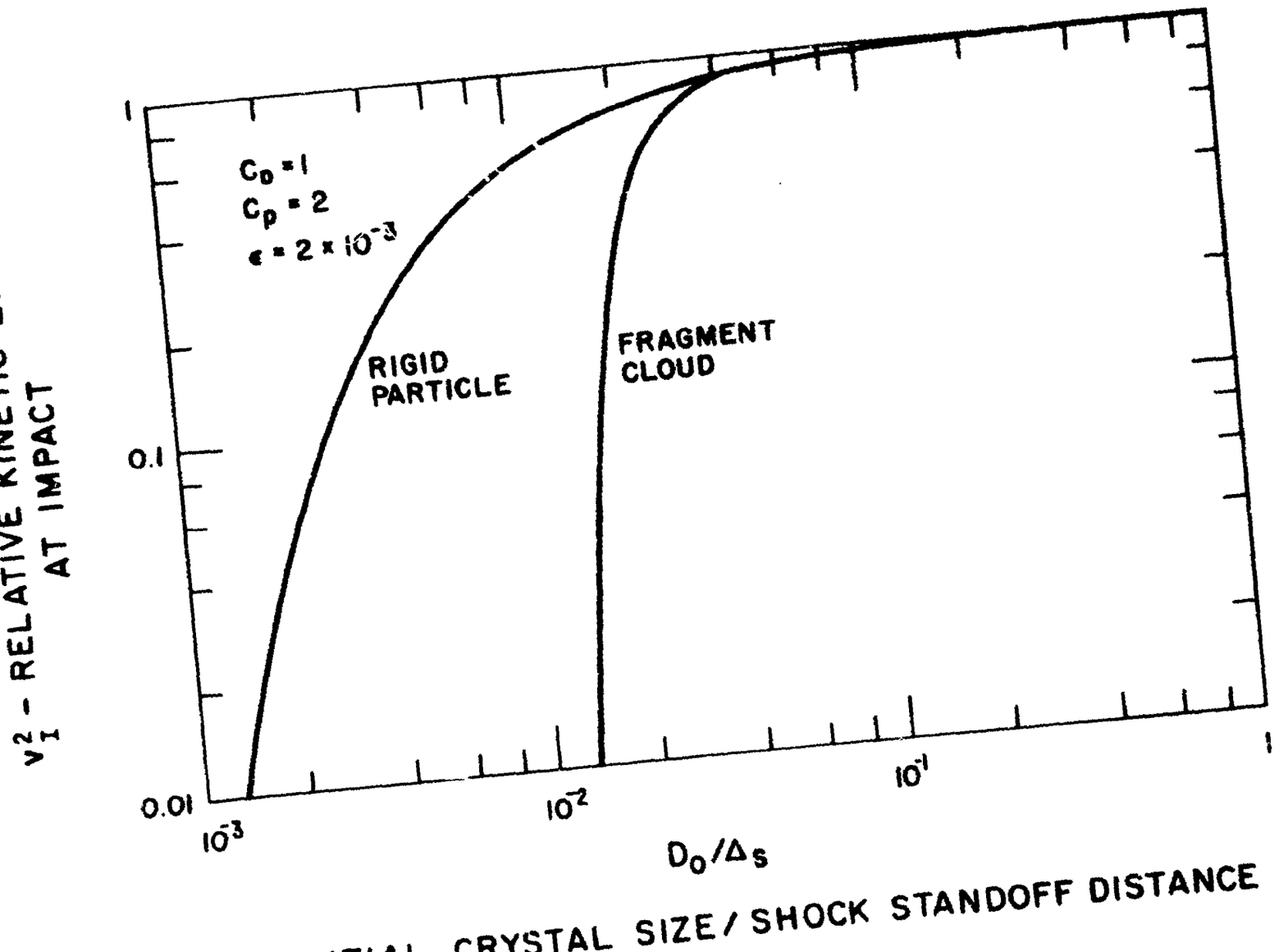

Fig. 17 Comparison of Impact Kinetic Energy

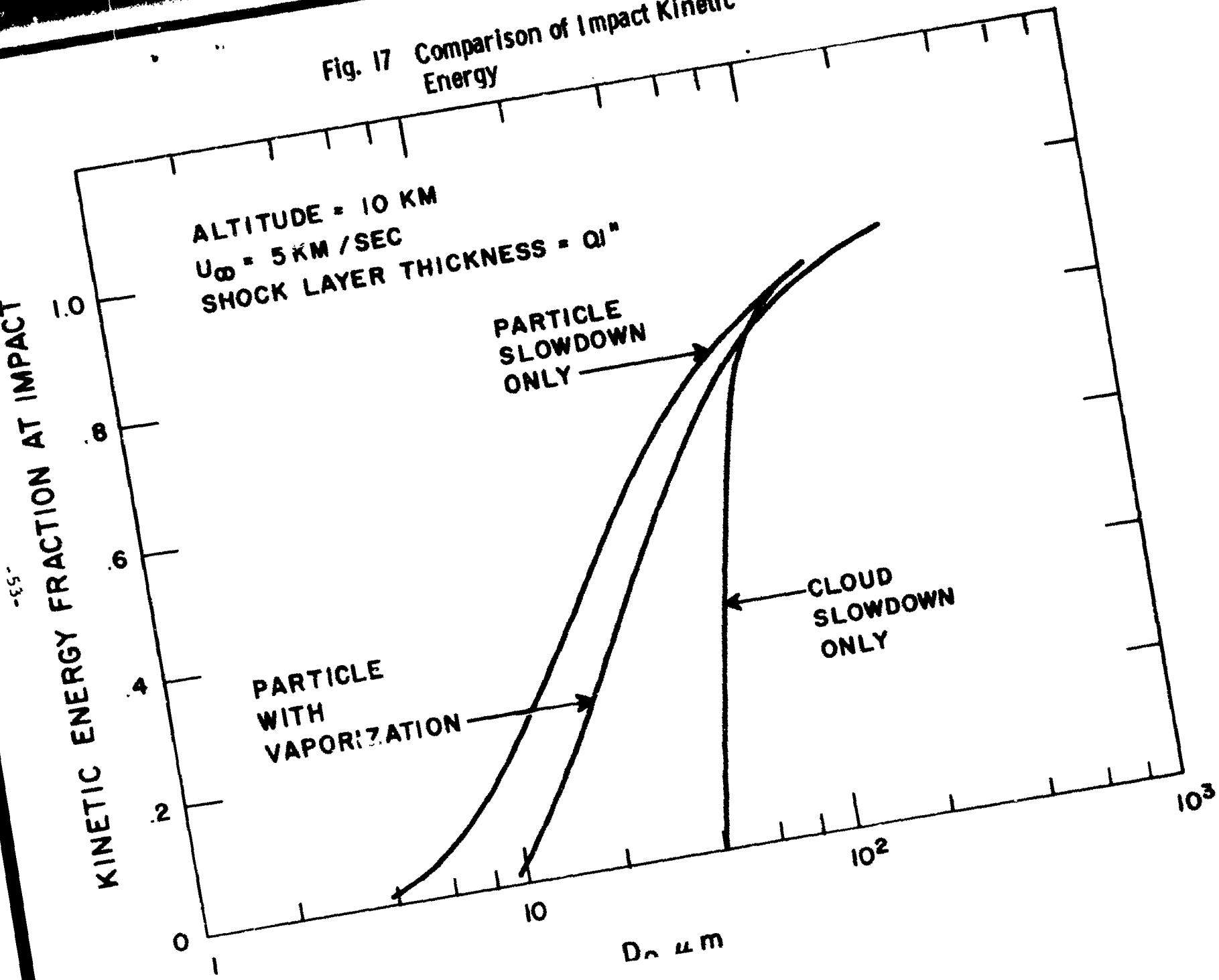

V. CONCLUSIONS

The problem of ice crystal impact with a hypersonic vehicle has been addressed. The conditions under which the ice crystal will fracture at the vehicle shock have been determined. A dynamic fracture criterion, which is subject to experimental verification, has been developed to determine the size and velocity of the crystal fragments. Using the initial fragment size and velocity from the model for dynamic fracture, it has been shown that the outer fragments continue to fracture and prevent the shock layer gas from penetrating the fragment cloud. Thus, the fragment cloud may be treated as a separate incompressible fluid without surface tension. The dynamics of the fragment cloud is then modeled by extending the Reinecke-Waldman[5] model for liquid drop deformation. The lateral spreading of the fragment cloud may significantly reduce the ice crystals impact velocity on the hypersonic vehicle. It is shown that the minimum tolerable fragment cloud may be an order of magnitude greater in size than the minimum tolerable rigid particle impacting the vehicle along the same stagnation point trajectory. Thus, the fracturing of the ice crystals at the vehicle shock may significantly reduce the erosion of the vehicle.

REFERENCES

1. R. F. Probstein and F. Fassio, "Dusty Hypersonic Flows," AIAA Journal, Vol. 8, No. 4, April 1970, P 772.

2. O. G. Engel, "Fragmentation of Waterdrops in the Zone Behind An Air Shock," Journal of Research of the NBS, Vol. 60, No. 3, March 1958.

3. A. Hanson, E. Domich, and H. Adams, "Shock Tube Investigation of the Breakup of Drops by Air Blasts," The Physics of Fluids, Vol. 6, No. 8, August 1963, pp. 1070-1080.

4. A. A. Ranger and J. A. Nicholls, "Aerodynamic Shattering of Liquid Drops," AIAA Journal, Vol. 7, No. 2, February 1969.

5. W. Reinecke, and G. Waldman, "An Investigation of Water Drop Disintegration in the Region Behind Strong Shock Waves," Proceedings of the Third International Conference on Rain Erosion and Related Phenomena, Hartley Whitney, Hampshire, England, August 1970.

6. G. D. Waldman and W. G. Reinecke, "Particle Trajectories, Heating, and Breakup in Hypersonic Shock Layers," AIAA Journal, Vol. 9, No. 6, June 1971, pp. 1040-1048.

7. E. Y. Harper, G. W. Grube and I-Dee Chang, "On The Breakup of Accelerating Liquid Drops," J. Fluid Mech., Vol. 52, Part 3, 1972, pp. 565-591.

8. P. G. Simpkins and E. L. Bales, "Water-Drop Response to Sudden Accelerations," J. Fluid Mech., Vol. 55, Part 4, 1972, pp. 629-639.

9. G. D. Waldman, W. G. Reinecke, and D. C. Glenn, "Raindrop Breakup in the Shock Layer of a High-Speed Vehicle," AIAA Journal, Vol. 10, No. 9, September 1972, P. 1200.

10. N. A. Jaffe, "Droplet Dynamics in a Hypersonic Shock Layer," AIAA Journal, Vol. 11, No. 11, November 1973, P 1562.

11. W. G. Reinecke and G. D. Waldman, "Shock Layer Shattering of Cloud Drops in Reentry Flight," AIAA Paper No. 75-152, Pasadena, Calif., January 1975.

12. M. L. Finson, P. F. Lewis, P. K. S. Wu, J. D. Teare, A. N. Pirri and P. E. Nebolsine, "Advanced Reentry Aeromechanics, Interim Scientific Report," Physical Sciences Inc., PSI TR-10, August 30, 1974.

13. D. J. Perry, Aircraft Structures, 1950, McGraw-Hill, pp. 88-96.

14. KH. A. Rakhmatulin and YU. A. Dem'Yanov, Strength Under High Transient Loads, 1961, S. Monson, Jerusalem and Wiener Bindery Ltd., Jerusalem, 1966, p. 81.

15. F. L. Singer, Strength of Materials, 2nd ed. 1962, Harper & Brothers, New York, p. 471.

16. C. Kittel, Introduction to Solid State Physics, 3rd ed. 1966, John Wiley & Sons, Chapter Five.

ACKNOWLEDGMENT OF SPONSORSHIP

Research jointly sponsored by the Space and Missile Systems Organization and the Air Force Office of Scientific Research (AFSC), United States Air Force, under Contract F44620-74-C-0022. The United States Government is authorized to reproduce and distribute reprints for governmental purposes notwithstanding any copyright notation hereon.